Clustering and Informative Path Planning for 3D Gas Distribution Mapping: Algorithms and Performance Evaluation

Chiara Ercolani, Lixuan Tang, Ankita Arun Humne, and Alcherio Martinoli

***Abstract*—Chemical gas dispersion can represent a severe threat to human and animal lives, as well as to the environment. Constructing a map of the distribution of gas in a fast and reliable manner is critical to ensure accurate monitoring of at-risk facilities and coordinate targeted and swift rescue missions when an emergency occurs. In recent years, robots have been endowed with gas sensing capabilities, and several algorithms to generate gas maps have been studied, often producing a 2D map. Two of the major drawbacks of these studies are concerned with the fact that the robot's path is often fixed to a predefined route, and that the tridimensionality of the gas dispersion phenomenon is not captured by the final gas maps. In this paper, we study the effect of a random walk and an adaptive path planning approach based on informative quantities to gas mapping in a 3D environment using a micro aerial vehicle with severe flight time constraints. We also introduce a clustering strategy to enhance the exploration of the environment. The strategies are compared to a lawnmower movement and evaluated against a ground truth map of the environment, both in simulation and with physical experiments, in order to assess which ones are able to provide an accurate gas map, while simultaneously achieving satisfactory coverage of the desired volume under time constraints.**

***Index Terms*—Aerial Systems: Applications, Environment Monitoring and Management, Reactive and Sensor-Based Planning**

I. INTRODUCTION

THE uncontrolled dispersion of chemical compounds in warehouses, chemical plants and during environmental emergencies can pose a considerable threat to both human lives and the environment. Research in the field of Gas Distribution Mapping (GDM) aims at constructing a map of the gas distribution in a given environment, drawing important conclusions about the presence of leaks, their location and the identification of areas presenting higher gas concentration. These techniques are also useful when monitoring sites where contamination of the air is unavoidable, to prevent exposure to excessive amounts of hazardous substances. Recent advances in the fields of embedded systems and chemical sensing allow GDM to be performed by robotic platforms, reducing the exposure of humans and animals to dangerous gases. Robotic GDM has been carried out primarily using ground robots [1]–[3] or flying vehicles whose movement is constrained to a 2D plane [4], [5]. However, since gas dispersion is inherently a 3D phenomenon, a recent research direction aims at extending the coverage to a tridimensional space, in order to increase the amount of information provided by the final map.

Unmanned Aerial Vehicles (UAVs), equipped with sensing capabilities, are employed for the tasks of GDM and Gas Source Localization (GSL) [5]–[9]. The biggest challenge when using UAVs arises from the turbulence generated by their propellers, called wake, which hinders gas detection [10], [11]. Nano Aerial Vehicles (NAVs, up to 15cm according to [12]) maintain similar flight dynamics properties to bigger drones, but the smaller propeller size generates a narrower wake, which does not hinder gas detection as much, particularly in indoor applications [4], [13], [14]. However, NAVs suffer from severe flight time constraints, a limitation that must be accounted for when planning gas detection missions with them.

One of the earlier works in the domain of GDM is reported in [15] and uses concentration grid maps with mobile robots to model the gas distribution. Plume mapping strategies based on Hidden Markov Methods (HMM) were proposed by Farrell et al. in [16]. Blanco et al. propose an approach based on a Kalman Filter for GDM [17]. Gaussian Processes (GP) have also been used for GDM [18], [19]. Additionally, a Gaussian Markov Random Field (GMRF) method has been proposed in [20], giving promising results. This method is suitable for cluttered environments, but is computationally expensive and does not scale well with larger maps.

The Kernel DM+V method presented in [21] aims at learning a statistical 2D gas distribution model from a sequence of localized gas sensor measurements. The method provides the mean of the gas distribution as well as its variance, and it offers a much less computationally expensive alternative compared to GP or GMRF methods. This method was used to create gas distribution maps with flying vehicles moving on a 2D plane in [5] and [22].

The Kernel DM+V was extended to provide 3D gas maps in [1], using a ground robot equipped with three sensors at different heights for the experimental validation. Later, the 3D Kernel DM+V/W method was implemented on a Micro Aerial Vehicle (MAV), namely a quadrotor of 50 cm of diameter, in [8]. Although this work pioneers the creation of a 3D gas distribution map with a UAV, the approach requires the path of the robot to be planned ahead. Moreover, a lack of in-depth

Manuscript received: September 9, 2021; Revised December 21, 2021; Accepted January 27, 2022. This paper was recommended for publication by Associate Editor B. Duncan and Editor P. Pounds upon evaluation of the reviewers' comments. This work was supported by the Swiss National Science Foundation under grant 200020_175809/.

All authors are with the Distributed Intelligent Systems and Algorithms Laboratory (DISAL), School of Architecture, Civil and Environmental Engineering, École Polytechnique Fédérale de Lausanne (EPFL), 1015 Lausanne, Switzerland, firstname.lastname@epfl.ch

experimental analysis makes it hard to assess the quality of the results. The drone performed two sweeps at 30 and 100 cm of height without stopping, due to flight time constraints. The fact that long stops to gather information are not strictly needed is also supported by [4], where a method is presented to localize the gas source from a gas map in a short time with measurements acquired in motion by a NAV.

Informative Path Planning (IPP) consists in designing path planning algorithms that aim at maximizing the amount of information gathered about a phenomenon, given some budget constraints. IPP strategies have been used, among other fields, to provide effective navigation strategies while estimating environmental quantities [23]. UAVs have been employed, for example, in [24], where IPP strategies based on entropy and mutual information improved the estimation of a temperature field, while [25] presented an IPP framework for UAV-based terrain monitoring.

In the field of GDM, path planning is usually done in a non-adaptive way following a predefined trajectory, often consisting of a sweeping motion path coupled with long stops at each measurement location [4], [5], [8]. An IPP approach was used for GDM in [22], where a comparison between a map constructed using a predefined sweeping strategy and one using an adaptive sensing strategy based on Artificial Potential Fields (APF) was carried out. Results show that the latter approach creates a meaningful map more quickly, which constitutes a big advantage given the limited flight time of a UAV. The biggest drawback of this IPP strategy is that its outcome depends greatly on the choice of coefficients for the APF, which have to be tweaked for each platform or environment, making this approach hard to generalize. IPP strategies for gas mapping have also been discussed in [26]. However, they have only been tested in a simulated 2D map.

Applying IPP algorithms to GDM presents some peculiar challenges due to the stochastic and time variant nature of the phenomenon, and the direct interaction between the robotic platform and the gas plume. Additionally, when employing a UAV, the wake of the propellers hinders sensing and provides less precise information for the IPP algorithms to use. The bounded flight time of a quadrotor is also an important limiting factor because it imposes additional constraints on the pace at which the map is composed and on the total information gathered.

In this paper, we couple three path planning strategies to a GDM algorithm and we compare their performance to a baseline widely used in literature. Two of these strategies are based on IPP, while the third consists of a type of random walk called Lévy flight. Subsequently, we apply a clustering method to the environment, with the objective of enhancing exploration, and we evaluate its effect on the three strategies. Due to its light computational requirements and good real-time performance, the 3D Kernel DM+V/W was used to create a 3D gas map. The resulting maps are evaluated by comparing them to the ground truth gas map of the environment. An NAV moving continuously in the environment is used to sense gas particles. The continuous movement allows the vehicle to fully take advantage of its mobility within the flight time constraints, while still producing meaningful results. While all the approaches presented in this paper are tested only in a quasi-laminar flow regime, they make no assumptions about the number of gas sources or their location and can therefore be employed in a wide variety of scenarios. The contributions of the paper are the following:

- The implementation of adaptive path planning techniques based on IPP to 3D GDM;
- The accurate evaluation of these techniques based on the ground truth gas map of the environment;
- The introduction of a clustering method to improve exploration of the environment, and the study of its effects on the mapping performance.

II. Approach and Algorithms

This section presents the algorithms used for GDM and for path planning, as well as the method used for ground truth acquisition. Moreover, it briefly introduces the reader to the robotic platform employed for this work. For all the strategies presented below, the experimental area is divided into a grid map of N cells.

A. Gas Distribution Mapping

The 3D Kernel DM+V/W algorithm introduced in [1] was used to produce a gas map of the environment. This algorithm uses a multivariate Gaussian weighting function to construct a map with the gas samples coming from the NAV. Additionally, the algorithm uses wind information from an on board anemometer. For this work, the wind information was provided a priori, since the intensity and direction of the wind are known throughout the experiments. For each cell $k \in N$, the weights are computed by evaluating a Gaussian kernel at the distance between the location of the measurement μ_i and the center $x^{(k)}$ of cell k:

$$w_i^{(k)} = \mathcal{N}(|x^{(k)} - \mu_i|, \sigma_0) = \frac{1}{(2\pi)^{\frac{3}{2}}|\Sigma|^{\frac{1}{2}}} e^{-\frac{1}{2}(x^{(k)}-\mu_i)^T \Sigma^{-1}(x^{(k)}-\mu_i)} \quad (1)$$

The covariance matrix Σ dictates the shape of the kernel and depends on the kernel width σ_0 and the stretching coefficient γ (they determine the amount of extrapolation on individual readings and the uncertainty related to the wind estimate, respectively), as well as on the wind velocity. For more information, please refer to the original 3D Kernel DM+V/W paper [1].

Additionally, the 3D Kernel DM+V/W algorithm provides a confidence map, indicating high confidence for a cell if a large number of readings was taken near its center. This feature was not used because the confidence value was consistently very low, since the navigation strategy of the NAV consists of a continuous movement, preventing a large amount of samples to be gathered in each grid cell. The quality of the map is instead evaluated against a ground truth after the experiments.

1) Ground truth acquisition: The ground truth data was acquired using an array of static sensors mounted on a traversing system (a 3-axis robotic manipulator present in many wind tunnels). The type of gas sensor mounted on the static sensors is the same one used by the NAV. The sensors sample at 10

Hz for a duration of 2 seconds at the center of each grid cell. After eliminating the outliers, the data obtained is averaged to produce the ground truth.

Even though the same type of sensor was used for ground truth acquisition and for experiments, calibration was necessary due to the small manufacturing differences introduced by each sensor. A linear regression model was used to describe the relationship between the data coming from each sensor node and the data coming from the NAV's sensor, while moving on a predefined path which traverses the plume.

2) Kernel parameters selection: In order to minimize the estimation error of the 3D Kernel DM+V/W algorithm, the key parameters σ_0 and γ have been optimized with a randomized search consisting of 1000 iterations in predefined intervals for the two parameters. To achieve this, the ground truth data was fed to the 3D Kernel DM+V/W algorithm in order to produce a map, and the parameters that minimized the Root Mean Square Error (RMSE) of the generated map were chosen to be used during experiments.

B. Path Planning

Given the flight time limitations of the platform employed for this work, navigation strategies that rely on stopping at each waypoint to gather data are not feasible. Moreover, only one Volatile Organic Compounds (VOC) sensor is mounted on the NAV, allowing it to obtain information about the distribution that affects only a small area around the robot. This prevents the mapping algorithm from drawing conclusions about the gas distribution in parts of the map that are far from the NAV's path. For these reasons, strategies that focus on the continuous movement of the robot are essential.

Two strategies based on informative quantities have been implemented. The first one is based on entropy, an information theoretic quantity widely used in IPP. The second one is based on the Kullback-Leibler Divergence (KLD) [27]. The third strategy consists of a type of random walk called Lévy flight. These three strategies are evaluated with and without the addition of the clustering method described in Section II-C. The lawnmower movement is used as a baseline.

1) Baseline: The lawnmower movement was previously used in several GDM papers [4], [5], [8] as a non adaptive path planning strategy. In this work, we reconstruct a gas map on five layers in the Z axis. In order to allow the lawnmower movement to cover the whole volume in the X direction within the time budget limits, the zig-zag trajectory is carried out only on three out of five planes (top, middle and bottom). Nonetheless, the 3D Kernel DM+V/W algorithm is able to extrapolate the value of the gas map at a maximum distance r_{co} from the locations where the measurements are taken, thus estimating the value of the gas concentration on the two layers where the robot does not directly navigate.

2) Lévy Flight: The Lévy flight is a type of random walk commonly used in robotics applications. This walk was chosen because the probability of returning to the previous position is smaller compared to other random walks [28].

3) Entropy Strategy: Entropy is an information theoretic quantity which measures the uncertainty in a random variable. For a given discrete random variable, entropy is computed as:

$$H(X) = -\sum_{n=1}^{N_b} P(X = x_n) log(P(X = x_n)) \tag{2}$$

where H is the entropy and x_n are the possible outcomes, in this case gas concentration values, which occur with probability $P(X = x_n)$. To compute the entropy for each grid cell, the gas sample values, previously normalized during the mapping step, are discretized by dividing them into N_b bins in order to ease computation.

The IPP strategy based on entropy proposed in this paper sets as next goal for the drone the unvisited grid cell with the maximum entropy to distance ratio, hence maximizing the following objective:

$$r_H = _{j \in \mathcal{N}} \left(\frac{H(X)_j}{d_{ij}} \right) \tag{3}$$

where i is the current position. Since all grid cells are initialized with a uniform probability distribution, whose entropy value is equally high among the unvisited ones, dividing the entropy by the distance can privilege shorter movements, forcing the drone to proceed gradually and preventing a zig-zag trajectory throughout the whole map. This behavior should be avoided given the flight time constraints of the drone and the additional turbulence caused by multiple passages in the same zone.

4) Kullback-Liebler Divergence Strategy: The KLD is an information theoretic quantity that measures the difference between two probability distributions, P and Q [27]. It has already been employed in literature as part of reward functions for gas sensing tasks [29]. It is computed as:

$$D_{KL}(P||Q) = \sum_i P(i) log_2 \left(\frac{P(i)}{Q(i)} \right) \tag{4}$$

For each grid cell, the KLD strategy compares the probability distribution P, obtained by the samples gathered in that grid cell, and the estimated probability distribution of the next step Q. All cells are initialized with a uniform probability distribution, which gets updated by the 3D Kernel DM+V/W algorithm. The distribution Q is obtained by adding one virtual sample i, corresponding to the current expected value of the distribution, to P and computing the new probability distribution. The larger the KLD, the more P and Q differ, indicating that the samples taken so far are not homogeneous in value. Therefore, the NAV should further explore the area and gather more samples to increase the confidence of the estimation. This strategy consists in setting as next goal the cell that has the highest value according to the following criterion:

$$r_{KLD} = _{i \in \mathcal{N}} \left(KLD_i \right) \tag{5}$$

This strategy does not require a normalization by distance because it inherently does not exhibit a zig-zag behavior.

C. Clustering Strategy

Mapping the gas distribution throughout an entire volume requires the whole space to be thoroughly visited. In particular,

when relying on IPP quantities, the stochastic nature of the phenomenon often hinders exploration and can lead the robot to proceed slowly and get stuck in areas of high gas variability, which often corresponds to high gas concentration. Moreover, employing a vehicle with propellers makes gas detection more difficult, affecting the performance of approaches based on quality and quantity of information gathered. To address these shortcomings, we developed a clustering strategy which divides the space in clusters and allows the drone to visit each cluster subsequently in a pre-planned order. Within each cluster, the drone is driven by the planning strategies mentioned in Section II-B.

Initially, the volume is divided into K clusters using the K-Means algorithm. This is achieved by randomly initializing the centroids of the K clusters, then repeatedly assigning each grid cell to the closest cluster using the L_2 distance and recomputing the centroids of each cluster. This operation is repeated until the centroids of the clusters do not change.

A Dynamic Programming (DP) algorithm is used to optimize the path between the centroids of the clusters, described as a Travelling Salesman Problem. This algorithm can find the globally optimal path and has complexity of $\mathcal{O}(2^K * K^2)$, requiring more computational effort and more time with a higher number of clusters. The order in which the drone will go through the clusters is decided a priori, to minimize time spent on transitions from one cluster to another.

For the Lévy flight, the algorithm will pick the first destination cell in each cluster at random and will subsequently use the Lévy flight to navigate within the cluster. For the Cluster Entropy and KLD methods, the first cell is picked using the r_H criterion, while the following cells are picked using r_H and r_{KLD} respectively. The same criterion is employed to select the initial cell because it allows the robot to exploit informative quantities when available, while privileging shorter steps.

The time allocated to the exploration of each cluster, T_c, is computed as the remaining flight time divided by the number of unvisited clusters. When the time spent in the current cluster t is greater than $0.8 * T_c$, if the proportion of updated cells containing gas falls below a threshold, the robot is prompted to choose a new cluster. This exit strategy allows for allocating more time to clusters containing more gas, while still maintaining a good exploration of the whole volume. If the percentage of updated cells containing gas continues to be above the threshold, the drone will continue exploring the cluster until the allocated cluster time elapses. This exit strategy is not based on informative quantities in order to extend its application beyond IPP approaches.

D. NAV Platform

The NAV used in this paper is a Crazyflie V2.1 (CF2, Bitcraze AB, Malmö, Sweden) equipped with a custom Printed Circuit Board (PCB) which provides gas sensing capabilities (see Figure 1). The PCB hosts a MICS-5521 CO/VOC sensor [30] and an STM8L151F3U6TR ultralow power microcontroller used to convert the analog data coming from the sensor to a digital format with a sampling frequency of 10 Hz. Previous work [13] has shown that placing the gas sensor

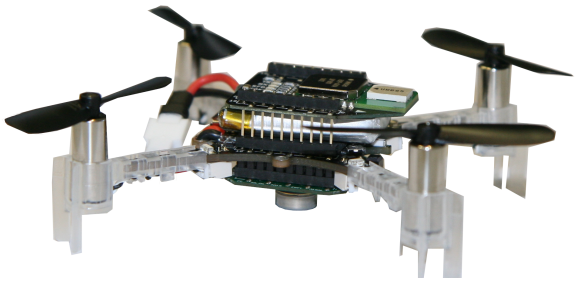

Fig. 1. Crazyflie V2.1 equipped with a custom PCB for gas sensing at the bottom.

at the bottom of the NAV enhances its sensing capabilities. This was the configuration chosen throughout this paper.

Localization is achieved with a Motion Capture System (MCS) from Motion Analysis[1] consisting of 13 Kestrel 1300 cameras. Five passive markers with an 8 mm diameter are placed on the CF2. The total weight of the payload is 6.5 g, which includes the custom PCB and the five MCS markers. Throughout all the experiments, the NAV is moving at a constant velocity of 0.15 m/s for a total flight time of 4 minutes and 30 seconds for each experiment. These values were chosen in accordance to the properties and limitations of the NAV. Additionally, the velocity was chosen to allow the CF2 to gather enough samples within a grid cell while guaranteeing a reasonable speed for exploration. The CF2 communicates with the ground station (a PC equipped with a USB antenna) over the 2.4 GHz ISM radio band. The position data is acquired by the MCS software and sent to the CF2 through the radio link. Algorithmic computations are also performed off-board.

III. PERFORMANCE EVALUATION

We first evaluated the strategies in a high-fidelity simulation, and then with physical experiments with the CF2 in our wind tunnel facility. This section describes the evaluation metrics used, the parametric choices carried out for the experiments, and the simulation and experimental setups.

A. Evaluation Metrics

Three metrics are used to quantify the performance of the different strategies presented in this paper: RMSE, coverage and shape coverage.

The RMSE was used to quantify the difference between the final gas map obtained with the 3D Kernel DM+V/W algorithm in combination with the IPP strategies and the ground truth. It is computed as:

$$RMSE = \sqrt{\frac{\Sigma_{i=1}^{N}(d_i - g_i)^2}{N}} \tag{6}$$

where d_i is the obtained gas value of each grid cell, g_i is the corresponding ground truth value and N is the total number of grid cells.

The coverage metric evaluates how much exploration was accomplished by each strategy. It is defined as the number of

[1]https://www.motionanalysis.com/

cells whose gas value has been updated over the total number of cells:

$$C = \frac{\#\ updated\ cells}{\#\ cells} \tag{7}$$

In this paper, we introduce the shape coverage metric, which represents the probability of an updated cell to be identified correctly as containing gas or not according to the ground truth, and is computed as:

$$SC = p(d_i \geq th_d | g_i \geq th_g || d_i < th_d | g_i < th_g)\ \forall i \in N_u \tag{8}$$

where th_d and th_g are the thresholds used to determine whether or not a cell contains gas and N_u is the number of updated cells. In simulation, $th_d = th_g$ and can be determined easily, since cells with no gas have a value close to 0. For the real experiments, since the sensitivity of sensors varies significantly due to environmental factors, thresholds are different for each map and are determined by considering areas with the lower 15 percent of the gas map readings as no gas zones and the upper 85 percent as gas zones. In fact, the stochastic nature of gas dispersion coupled with the propeller perturbation makes it hard to establish a threshold that is valid for all runs.

To ease the comparison between the different methods, the metrics are combined in one overall metric:

$$M = SC * C * |1 - RMSE| \tag{9}$$

Higher values of this metric indicate better performance of the algorithm.

B. Algorithmic Parameters

The parameters chosen for the 3D Kernel DM+V/W mapping algorithm can be seen in Table I. Parameters σ_0 and γ were computed with a random search, as described in Section II-A, after fixing the value of r_{co} to 0.3m. This is the radius within which the cells are affected by a gas sample. Coincidentally, the relationship between σ_0 and r_{co} is the same as the one reported in [1]. Additional parameters reported in Table I are the total number of cells, N and the size of each cell, which is the same in all three dimensions.

TABLE I
PARAMETERS FOR THE 3D KERNEL DM+V/W ALGORITHM

N	cell size	σ_0	γ	r_{co}
7000	0.1m	0.1	83	0.3m

These parameters were found using real data and are also used in simulation, since they were giving good results.

The choice regarding the number of clusters was taken using simulated data and is described in the next section.

C. Simulation Setup

Webots [31], a high-fidelity open-source simulator, was used for the simulation experiments. An odor dispersion plugin [32] was used to provide an acceptable simulation of the wind and gas fields. A simulated Crazyflie equipped with a gas sensor was also used in the simulation. For each strategy, 10 experiments were run, each lasting 4 minutes and 30 seconds.

The biggest drawback of the simulator is that it does not take into account the effect of the wake of the propellers on the gas dispersion. In our previous work in [13], we demonstrated that the propeller to gas plume ratio of our setup allows for good gas detection. For this reason, we decided to use simulation to test our algorithms and draw some important conclusions about our methods that would require a too high volume of physical experiments otherwise. However, because of the difficulties in perfectly modelling the stochastic gas dispersion together with the wake effect, we always validate our simulated data with real experiments.

D. Wind Tunnel Setup

The experiments were carried out in a wind tunnel of volume 18x4x2 m^3. Inside the tunnel, the wind speed can be adjusted and is laminarized by a dedicated honeycomb filter. The volume of the tunnel effectively used for experiments is 7x2x0.5 m^3. Constraints on the volume are caused by the limited flight time of the experiments. Given the size and capabilities of the drone, this volume is comparable to the ones previously used in literature for GDM. The wind speed is kept at 0.7 m/s throughout all the experiments. Limitations in the testing regime employed in this paper could yield different results from experiments done in environments with higher turbulence or different gas dispersion rates.

The gas used during the experiments is ethanol, released by a stationary electric pumping device. The source release rate is set to 0.5 L/min, and corresponds to a mix of air and ethanol released by the pump. The environmental conditions chosen for this work are the ones that provided the best sensing results in the 3D GSL experiments presented in [13]. The initial position of the robot is the same for all approaches and corresponds to the right corner of the volume opposite to the source. For each strategy, ten experiments were carried out, each lasting 4 minutes and 30 seconds.

IV. RESULTS

This section presents and comments on the simulation and experimental results.

A. Simulation Results

The simulation results are presented in Figure 2. The lawnmower has remarkably consistent performance and outperforms the three other strategies when the whole area is considered to be one cluster, which is equivalent to saying that no clusters are used. Additionally, in this configuration, the Lévy flight outperforms the informative strategies.

When clusters are introduced, we can see that Lévy flight, Entropy and KLD outperform the lawnmower and their performance keeps improving the more clusters are used, plateauing at 15 clusters. It seems that adding more clusters beyond 15 helps to decrease the variability of the results.

Table II shows that all runs perform well in terms of shape coverage, which is explained by the good quality of the data

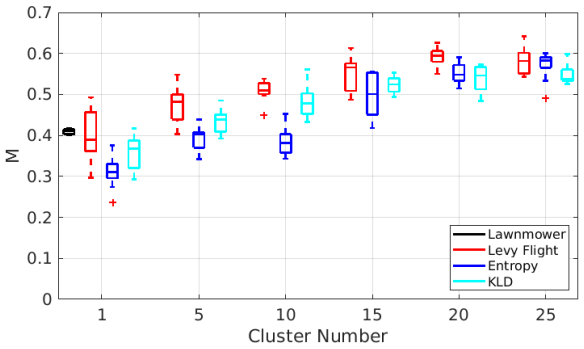

Fig. 2. Simulation results for the lawnmower baseline and for the three strategies with increasing number of clusters.

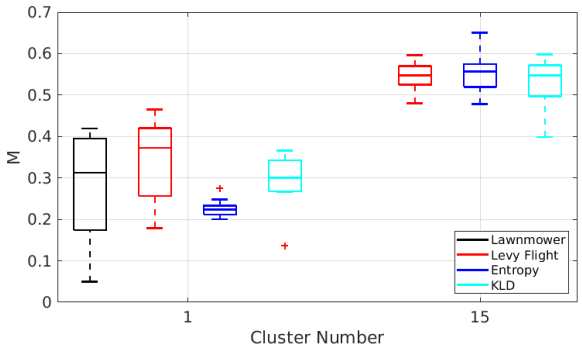

Fig. 3. Real experiment results for lawnmower and for the three strategies with 1 and 15 clusters

captured in simulation coupled with the effectiveness of the interpolation carried out by the 3D Kernel DM+V/W algorithm. The introduction of clusters improves the performance by greatly impacting the coverage metric, without significantly impacting the RMSE.

Based on the results from simulation, we decided to carry out real experiments with 15 clusters. This is the best trade-off between good performance in simulation, fast computation of the optimal path between clusters with the DP algorithm, and no excessive constraints on the navigation by having too small clusters.

TABLE II
EVALUATION METRICS - AVERAGE OF 10 RUNS IN SIMULATION

Strategy	RMSE	C	SC	M
Lawnmower	0.0509	0.5150	0.8369	0.4090
Lévy flight	0.0591	0.5136	0.8124	0.3925
Entropy	0.0536	0.4196	0.8228	0.3973
KLD	0.0539	0.4761	0.8178	0.4347
Lévy flight + 15 Clusters	0.0565	0.7235	0.8128	0.5554
Entropy + 15 Clusters	0.0530	0.6618	0.7909	0.4966
KLD + 15 Clusters	0.0542	0.6923	0.7973	0.5220

TABLE III
EVALUATION METRICS - AVERAGE OF 10 RUNS IN THE REAL WORLD

Strategy	RMSE	C	SC	M
Lawnmower	0.0735	0.5471	0.5597	0.2837
Lévy flight	0.0749	0.4844	0.7595	0.3448
Entropy	0.0783	0.3777	0.6495	0.2263
KLD	0.0738	0.4924	0.6399	0.2932
Lévy flight + 15 Clusters	0.0624	0.7471	0.7775	0.5442
Entropy + 15 Clusters	0.0621	0.7550	0.7775	0.5505
KLD + 15 Clusters	0.0637	0.7346	0.7736	0.5322

B. Experimental Results

The results obtained with real experiments are presented in Figure 3. The real experiments present a general trend similar to the one outlined in simulation. The lawnmower outperforms the entropy strategy when the whole volume is considered to be one cluster. However, in real experiments, the KLD and Lévy flight strategies with one cluster perform similarly to the lawnmower. More insights to understand this performance can be gained by looking at Table III. Lawnmower, KLD and Lévy flight with one cluster have similar average RMSE, and lawnmower provides better coverage of the volume. However, the shape coverage is significantly worse for the lawnmower, not only compared to KLD and Lévy flight with one cluster, but in general. We can attribute this loss in performance to the effect of the propellers, which can be isolated in this instance thanks to the comparison to simulation, coupled with the movement of the drone, which is continuous and perpendicular to the plume. Other methods are more robust to this interference because they can compensate for the loss of sensitivity due to the propellers by not exclusively moving perpendicularly to the plume. It is worth highlighting that having the lawnmower move perpendicularly to the plume is consistent with the usage of this path planning method in literature. Additionally, KLD seems to outperform the entropy strategy on all metrics when only one cluster is used. This suggests that, in real experiments, the informative strategy based on KLD allows the robot to explore well, while delivering good quality of data.

Similarly to simulation, when clusters are introduced, an overall increase of performance can be observed. The breakdown of the metrics in Table III highlights that the introduction of clusters causes a consistent decrease in RMSE and increase in coverage and shape coverage, emphasizing a consistent improvement across all metrics due to increased exploration of the map. No significant differences are found among the performance of the three strategies coupled with clusters, suggesting that, given the difficulty of sensing gas with an NAV, adding a clustering method is what has the greatest impact on enhancing the final result.

The best maps obtained for each strategy according to the metric M, as well as the ground truth map, are displayed in Figure 4. The black areas indicate the parts of the map that were left unexplored. It can be clearly seen that the approaches coupled with clustering produce the best maps. Single cluster strategies also produce meaningful maps, but for a smaller area. This suggests that, with a higher time budget, the whole area would have been covered in a satisfactory way and with a high quality final map. The map produced when

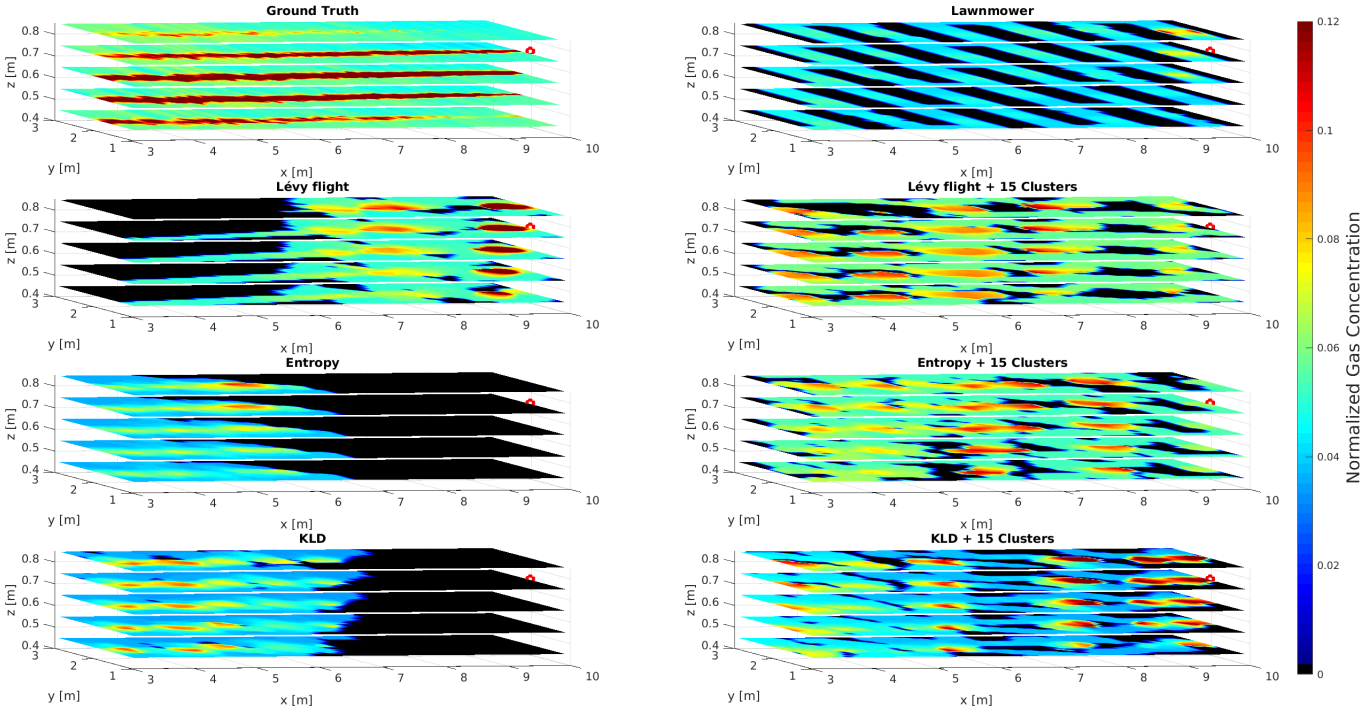

Fig. 4. Examples of maps produced by the 3D Kernel DM+V/W algorithm in real experiments, coupled with different path planning strategies. The ground truth map and the baseline are also depicted in the same scale. The source of the gas is marked with a red circle in each map. The dark blue areas indicate unexplored zones whose grid cells never got updated, while areas with no gas appear in light blue. All values are normalized against the maximum and minimum concentration values used for the 3D Kernel DM+V/W.

the robot follows the lawnmower movement clearly shows the limitations of the baseline. In fact, the resulting map consists of a sequence of stripes corresponding to the areas around the path of the robot. The size of the stripes is limited by the r_{co} of the 3D Kernel DM+V/W algorithm. One could obtain a smoother map by taking smaller steps in the X direction, but this would prevent from covering the whole volume. This map suggests that the lawnmower path does not scale well with larger volumes and produces patchier maps compared to other methods. Moreover, as suggested by the shape coverage metric, the shape of the plume is not well identified and there is less contrast between areas of gas and no gas compared to other approaches.

Pseudocolor plots of the gas maps at the inlet height obtained using the Lévy flight strategy with and without clusters, as well as the corresponding ground truth map, are shown in Figure 5. The cluster strategy allows for encompassing the whole shape of the plume more accurately and highlighting gaseous zones through the whole plane.

One interesting phenomenon can be observed in the maps for all approaches in Figure 4: significant gas patches are detected in the highest layer, in a stark contrast with the ground truth data. This could be an artifact of the 3D Kernel DM+V/W algorithm, coupled with the plume dispersion effect generated by the NAV's propellers. A similar phenomenon can also be noticed in Figure 5, where the reconstructed maps have slightly wider shapes compared to the ground truth. Further studies should investigate this phenomenon, as it might be an important aspect to factor in when producing 3D gas maps with the aid of a vehicle equipped with propellers.

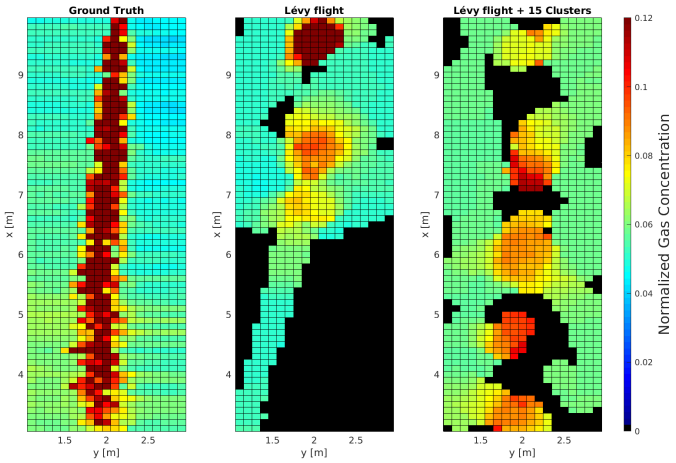

Fig. 5. Pseudocolor plots of the gas maps obtained with Lévy flight with and without clusters at z = 0.7 m, beside the corresponding ground truth map.

V. CONCLUSIONS AND OUTLOOK

In this paper, we evaluate the use of IPP and random walk strategies coupled with clustering to plan the 3D route of an NAV, while the robot performs a gas mapping task. The algorithm used to generate the gas map was the 3D Kernel DM+V/W algorithm, a widely used approach in GDM literature. The experimental evaluation was conducted with an NAV flying for 4 minutes and 30 seconds inside a wind tunnel.

GDM using drones is affected by difficulties in sensing due to the effect of the propellers on the plume, and by time constraints. Moreover, the stochastic nature of the phenomenon can lead traditional IPP strategies to focus too much on exploration of areas with high gas variability, while neglecting a sizeable portion of the environment. The comparison with simulation was able to highlight that the baseline lawnmower approach is not able to grasp the shape of the plume as well as other methods in physical experiments, because of the coupling of the impact of the propellers during data detection with its perpendicular movement to the plume. Strategies based solely on entropy and KLD, as well as the usage of Lévy flight, were able to provide high quality maps of a rather small area, since they do not favour exploration enough to achieve satisfying coverage under strict time constraints. Adding a clustering strategy delivers a reasonably accurate 3D map of a sizable environment compared to the size of the vehicle by greatly enhancing the exploration component of the gas mapping mission and increasing the quality of the gathered data.

Future work will focus on further improving the clustering strategies. Moreover, multi-robot strategies should be explored in order to improve coverage of all algorithms. Finally, these approaches could be employed in the development of a strategy that simultaneously localizes and maps the source.

REFERENCES

[1] M. Reggente and A. J. Lilienthal, "The 3D-kernel DM+V/W algorithm: Using wind information in three dimensional gas distribution modelling with a mobile robot," in *IEEE International Conference on Sensors*, 2010, pp. 999–1004.

[2] A. J. Lilienthal, A. Loutfi, J. L. Blanco, C. Galindo, and J. Gonzalez, "A Rao-Blackwellisation approach to GDM-SLAM: Integrating SLAM and gas distribution mapping (GDM)," in *3rd European Conference on Mobile Robots*, 2007, pp. 126–131.

[3] A. Gongora, J. Monroy, and J. Gonzalez-Jimenez, "Joint estimation of gas and wind maps for fast-response applications," *Applied Mathematical Modelling*, vol. 87, pp. 655–674, 2020.

[4] J. Burgués, V. Hernández, A. J. Lilienthal, and S. Marco, "Smelling nano aerial vehicle for gas source localization and mapping," *Sensors*, vol. 19, no. 3, Art. no. 478, 2019.

[5] P. P. Neumann, M. S. I. V. H. Bennetts, and I. M. Bartholmai, "Adaptive gas source localization strategies and gas distribution mapping using a gas-sensitive micro-drone," *Technology (BMWi)*, vol. 4, no. 5, Art. no. 6, 2012.

[6] M. Rossi, D. Brunelli, A. Adami, L. Lorenzelli, F. Menna, and F. Remondino, "Gas-drone: Portable gas sensing system on UAVs for gas leakage localization," in *IEEE International Conference on Sensors*, 2014, pp. 1431–1434.

[7] T. Kersnovski, F. Gonzalez, and K. Morton, "A UAV system for autonomous target detection and gas sensing," *IEEE Aerospace Conference*, 2017, DOI 10.1109/AERO.2017.7943675, (12 pages).

[8] L. Bing, M. Qing-Hao, W. Jia-Ying, S. Biao, and W. Ying, "Three-dimensional gas distribution mapping with a micro-drone," in *34th Chinese Control Conference*, 2015, pp. 6011–6015.

[9] M. Hutchinson, C. Liu, and W.-H. Chen, "Source term estimation of a hazardous airborne release using an unmanned aerial vehicle," *Journal of Field Robotics*, vol. 36, no. 4, pp. 797–817, 2019.

[10] M. Rossi and D. Brunelli, "Gas sensing on unmanned vehicles: Challenges and opportunities," in *IEEE New Generation of Circuits and Systems Conference*, 2017, pp. 117–120.

[11] T. Villa, F. Salimi, K. Morton, L. Morawska, and F. Gonzalez, "Development and validation of a UAV based system for air pollution measurements," *Sensors*, vol. 16, no. 12, a. 2202, 2016.

[12] M. Hassanalian and A. Abdelkefi, "Classifications, applications, and design challenges of drones: A review," *Progress in Aerospace Sciences*, vol. 91, pp. 99–131, 2017.

[13] C. Ercolani and A. Martinoli, "3D odor source localization using a micro aerial vehicle: System design and performance evaluation," in *IEEE/RSJ International Conference on Intelligent Robots and Systems*, 2020, pp. 6194–6200.

[14] S. Shigaki, M. Fikri, and D. Kurabayashi, "Design and experimental evaluation of an odor sensing method for a pocket-sized quadcopter," *Sensors*, vol. 18, no. 11, a. 3720, 2018.

[15] A. Lilienthal and T. Duckett, "Creating gas concentration gridmaps with a mobile robot," in *IEEE/RSJ International Conference on Intelligent Robots and Systems*, vol. 1, 2003, pp. 118–123.

[16] J. A. Farrell, S. Pang, and W. Li, "Plume mapping via hidden Markov methods," *IEEE Transactions on Systems, Man, and Cybernetics, Part B*, vol. 33, no. 6, pp. 850–863, 2003.

[17] J. L. Blanco, J. G. Monroy, A. Lilienthal, and J. Gonzalez-Jimenez, "A Kalman filter based approach to probabilistic gas distribution mapping," in *28th Annual ACM Symposium on Applied Computing*, 2013, pp. 217–222.

[18] M. Hutchinson, P. Ladosz, C. Liu, and W.-H. Chen, "Experimental assessment of plume mapping using point measurements from unmanned vehicles," in *IEEE International Conference on Robotics and Automation*, 2019, pp. 7720–7726.

[19] C. Stachniss, C. Plagemann, and A. J. Lilienthal, "Learning gas distribution models using sparse gaussian process mixtures," *Autonomous Robots*, vol. 26, no. 2, pp. 187–202, 2009.

[20] J. G. Monroy, J.-L. Blanco, and J. Gonzalez-Jimenez, "Time-variant gas distribution mapping with obstacle information," *Autonomous Robots*, vol. 40, no. 1, pp. 1–16, 2016.

[21] A. J. Lilienthal, M. Reggente, M. Trincavelli, J. L. Blanco, and J. Gonzalez, "A statistical approach to gas distribution modelling with mobile robots-the kernel DM+V algorithm," in *IEEE/RSJ International Conference on Intelligent Robots and Systems*, 2009, pp. 570–576.

[22] P. P. Neumann, S. Asadi, A. J. Lilienthal, M. Bartholmai, and J. H. Schiller, "Autonomous gas-sensitive microdrone: Wind vector estimation and gas distribution mapping," *IEEE Robotics & Automation Magazine*, vol. 19, no. 1, pp. 50–61, 2012.

[23] E. Galceran and M. Carreras, "A survey on coverage path planning for robotics," *Robotics and Autonomous Systems*, vol. 61, no. 12, pp. 1258–1276, 2013.

[24] W. C. Evans, D. Dias, S. Roelofsen, and A. Martinoli, "Environmental field estimation with hybrid-mobility sensor networks," in *IEEE International Conference on Robotics and Automation*, 2016, pp. 5301–5308.

[25] M. Popović, T. Vidal-Calleja, G. Hitz, J. J. Chung, I. Sa, R. Siegwart, and J. Nieto, "An informative path planning framework for UAV-based terrain monitoring," *Autonomous Robots*, vol. 44, no. 6, pp. 889–911, 2020.

[26] C. Rhodes, C. Liu, and W.-H. Chen, "Informative path planning for gas distribution mapping in cluttered environments," in *IEEE/RSJ International Conference on Intelligent Robots and Systems*, 2020, pp. 6726–6732.

[27] S. Kullback and R. A. Leibler, "On information and sufficiency," *The Annals of Mathematical Statistics*, vol. 22, no. 1, pp. 79–86, 1951.

[28] G. Viswanathan, V. Afanasyev, S. V. Buldyrev, S. Havlin, M. Da Luz, E. Raposo, and H. E. Stanley, "Lévy flights in random searches," *Physica A: Statistical Mechanics and its Applications*, vol. 282, no. 1-2, pp. 1–12, 2000.

[29] F. Rahbar, A. Marjovi, and A. Martinoli, "An algorithm for odor source localization based on source term estimation," in *IEEE International Conference on Robotics and Automation*, 2019, pp. 973–979.

[30] SGX Sensortech technologies, "MiCS-5521 CO/VOC sensor," https://www.sgxsensortech.com.

[31] O. Michel, "Cyberbotics ltd. Webots™: professional mobile robot simulation," *International Journal of Advanced Robotic Systems*, vol. 1, no. 1, pp. 39–42, 2004.

[32] Wikibooks, "Webots odor simulation — wikibooks, the free textbook project," https://en.wikibooks.org/w/index.php?title=WebotsOdorSimulation\&oldid=1966420, 2010, accessed: 2021-09-01.